Ice-Structureinteraction Under Hydrodynamic Loads of An Underwater Tankdedicated To the Intervention And Remediation of Trapped Pollutant in Tanker Wrecks

Dimitrios E. Mazarakos[a]*,Athanasios Kotzakolios[a],V. Kostopoulos[a]

[A] *Applied Mechanics Laboratory, Department Of Mechanical Engineering And Aeronautics, University Of Patras, Greece*
Corresponding Author: Dimitrios E. Mazarakos[a],*

---**ABSTRACT**--

A method for the prompt and cost-effective intervention and remediation of tanker wrecks has been proposed within the frame of the EU DIFIS project. The proposed concept relies on gravity forces to channel the flux of spilt fuel towards a buffer reservoir/separator, 30m below the sea surface, by means of a light, quickly deployable and flexible structure that should stay in place until the pollution threat is eliminated.

In this paper, the work on the survivability of two buffer bell reservoir material configurations (Aluminum and GFRP) against ice loading during the deployment phase of the system is summarized. The analyzed structure is a part of a double inverted funnel. This component, the buffer bell, is used for the temporary storing of the recovered oil and during the deployment procedure it is possible to be subjected to ice loading due to the operational environment of the structure. More specifically, two buffer bell configurations, regarding the materials, one made from aluminum and the other on from Glass Fiber Reinforced Plastic (GFRP) are investigated by using finite element analysis in LS-Dyna for the case were an ice sheet impacts the buffer bell. Two load cases were investigated relative to Buffer Bell's motion: a) a stationary condition (zero velocity) and b) motion due to sea waves and currents. The outcome of this analysis was to identify design issues and possible deployment/operation problems by predicting the damage location and extend. Structural stability issues are also considered.

Keywords: Ice-structure interaction, Finite element analysis, sea wave diffraction, Buffer Bell, DIFIS

Date of Submission: 25-11-2017   Date of acceptance: 22-12-2017


I.   INTRODUCTION

The analysis of underwater structures using the finite element method is a new way introduced in ship design, offshore and submarine engineering during the last years. The fluid/structure interaction between offshore structures and the sea environment (waves, currents, and ice) is an aspect analyzed by many researchers such as Chen and Mercier [[1]].The intervention of ice with offshore structures is a problem in which the platform piles must withstand the ice loads. The main modeling challenge of this interaction using numerical tools is to quantify a large number of parameters (structure's material and ice-sheet mechanical properties, ice velocity, size of ice- sheet). For this reason sets of experimental and environmental data are studied in order to define the sea conditions in which the ice sheet impacts the structure. These input data are used by the FE model and the impact forces are calculated. All these would improve the design and the total cost (especially at the construction phase) of the offshore and underwater structures.

II.   DESCRIPTION OF UNDERWATER STRUCTURE

The underwater structure consists of seven parts and is anchored on sea bed for oil recovery from shipwrecks. These parts are:

- The buffer bell (BB): A vessel made of aluminum and steel (external diameter 36m, length 39m) for the temporary storing of recovered oil.
- The riser tube(RT): A vertical polyethylene pipe (external diameter 2m, overall length 2000m) for the connection of the buffer with the dome and shipwreck
- The dome(DM): A conical shaped structure made of thin, flexible, lightweight cloth (base diameter 100m and height 100m) which covers the shipwreck and drives the collected oil to the buffer bell through the riser tube
- The dome interface unit (DIU): A conical substructure made of aluminum (base diameter 10m and height 10m) serving as a connection interphase between the riser tube and the dome structure.

- The mooring lines (ML) are flexible Dyneema cables [[2]] (Diameter 96mm and length 2000m) which support the riser tube and the dome, and are anchored to the seabed.
- The stiffening rings (SR) are steel disks (Diameter 4m and thickness 30mm) which connect the each part of the riser tube and connect them with the mooring lines.
- The anchoring system (AS): Twelve (12) deadweight cement anchors, holding the overall structure to the seabed.
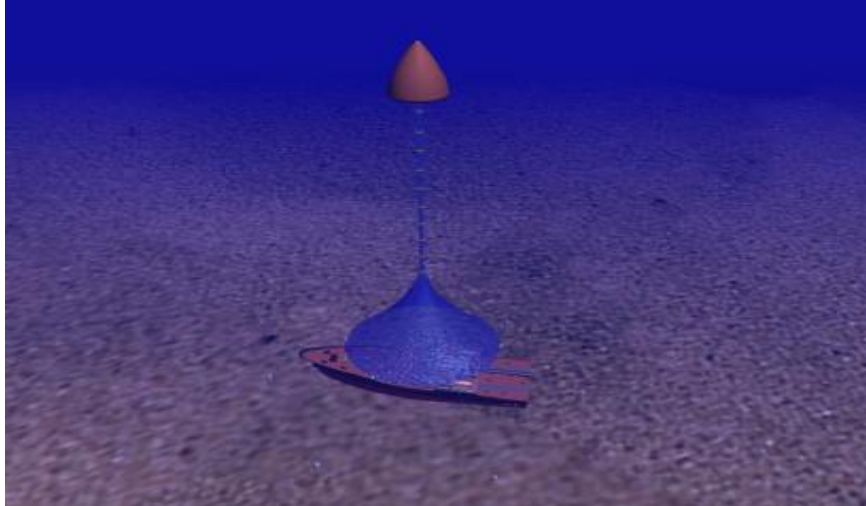
Figure 1: The underwater structure

At the operation phase, the buffer bell is the substructure that produces the upwards force (the difference between the buoyancy and the weight) tensioning the whole structure. The riser tube is connected to buffer bell by the mooring lines which run across the whole length of the tube through the stiffening rings, until they reach the dome interface unit. At this point, the DIU is secured between the Dome and the Riser Tube. The mooring lines run in periphery of the dome and finally attach to the deadweight anchors. In contrast to common offshore structures, this new design for oil recovery is not affected by weather conditions at the sea surface because it is fully submerged. So the structure should withstand only the hydrodynamic loads from sea currents and the high hydrostatic pressure due to the operational depth. This is an advantage because the system can remain submerged for long periods until complete oil recovery is accomplished.

III. DESCRIPTION OF BUFFER BELL (BB)

The buffer bell (BB) is a key element of this underwater structure, composed of two main parts: the upper and the lower. The first is an aluminum cylindrical structure and it is called capacitor. The capacitor is used as a temporary storage of the recovered oil. The second is an aluminum cubic structure, attached to the capacitor's external surface, and it is called floater. The floater is used for the production of upward force.
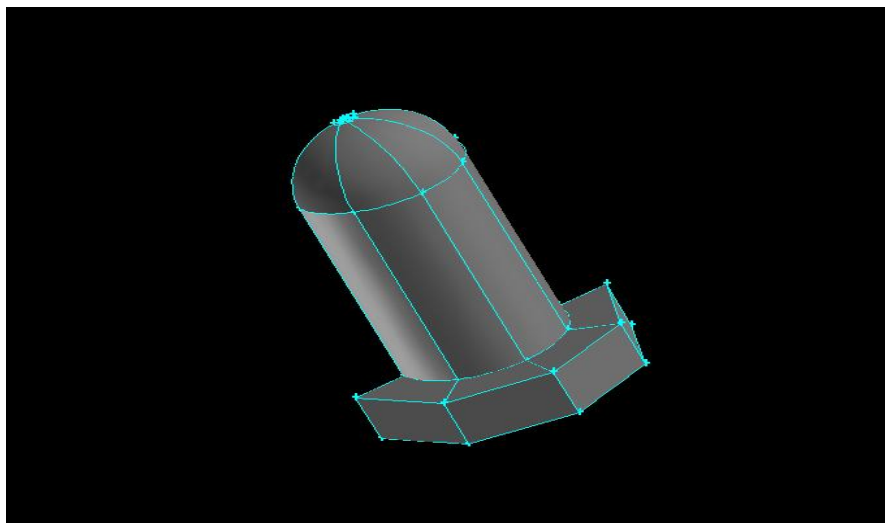
Figure 2: The buffer bell

The buffer bell's main dimensions are presented in Table 1:

Table 1: Buffer Bellmain dimensions

Buffer bell's part	Dimension	
Capacitor	Diameter(mm)	16000
	Cylinder height(mm)	25000
	Thickness(mm)	3
	Topsphere radius (mm)	8000
	Overall length(mm)	33000
	Capacity (m³)	5000
Floater	External Diameter (mm)	26000
	Internal Diameter (mm)	16000
	Height (mm)	6000
	Length(mm)	5000
	Buoyancy(tons)	1500
Center of gravity (CoG)	At the half of floater height	3000

These two parts are connected with mechanical joints and creates a continuous structure.

## IV.   DESCRIPTION OF BUFFER BELL'S DEPLOYMENT

During buffer bell's preliminary deployment studies, the previously mentioned parts are carried on a ship. During the erection the capacitor and the floater are joined together and the Buffer Bell structure is ready for installation. This phase in which all the components are being deployed under the sea is time dependent and weather conditions sensitive.

Actually calm weather conditions are demanded for successful installation. This time-consuming procedure starts with the DIU and dome placed close to the seabed with the mooring lines to the periphery. The mooring lines are connected to deadweight anchors on the seabed (downwards) and upwards with the surface ship that controls the tension forces and displacements. Then the riser tube is assembled and attached to the mooring lines through the SR's and then clamped to the dome interface unit. At this point the structure without the Buffer Bell is being attached to the surface ship through the mooring lines [[2]].
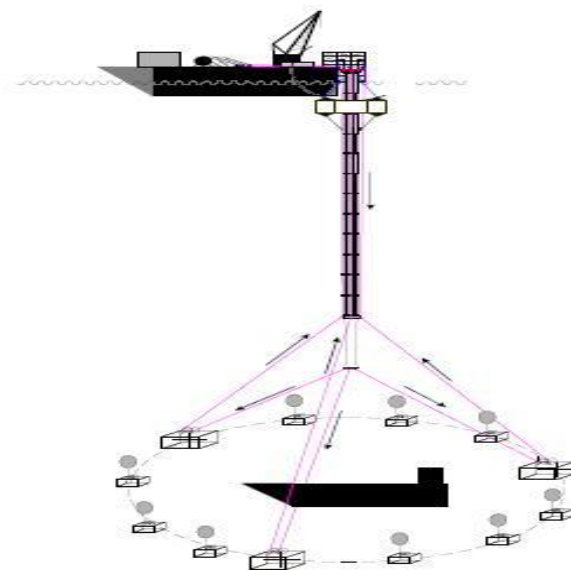
Figure 3: The structure deployment

The Buffer Bell is deployed last and two different scenarios can be applied. First, the floater can be ballasted with water in order to sink and reach the structure and then to be connected to the structure by Remote Operated Vehicles (ROVs) and second, the buffer bell is directly attached to the mooring lines and then all the components are sunk to the operational depth using underwater pulleys and forces from the surface ship.
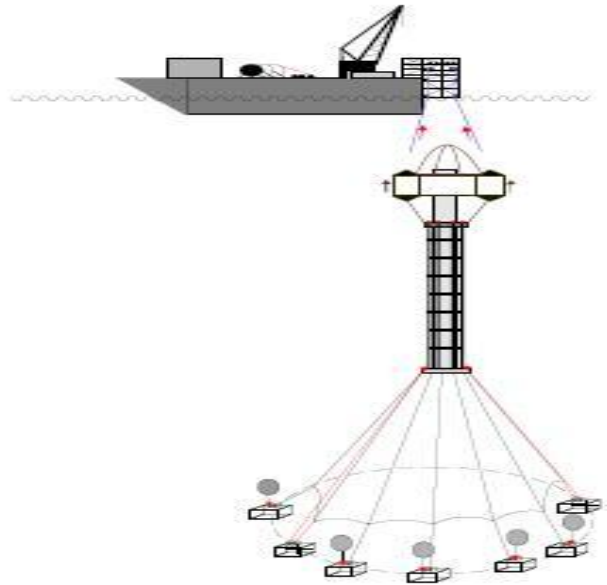
Figure 4: Buffer bell deployment

In current analysis the second scenario is considered and the overall structure is being deployed in a polar region such as the Baltic Sea, Arctic Ocean or Canadian coasts. When the Buffer bell is in the water (not ballasted) and connected to the mooring lines, and before it is placed to the operational depth (30 m below the sea surface), there is the possibility of being subjected to ice loading by a large ice sheet. This situation could be crucial for the structural integrity of the whole system. The capacitor could be damaged or a mooring line could fail from the impact forces and as a result the oil recovery procedure would be delayed.

V. THE SEA ICE

5.1 The Structure Of Ice
The ice consists of the same basic elements as ordinary water, i.e. hydrogen and oxygen. It is also consisted from many ice crystals sizing from less than 1mm to several millimeters. The geometrical structure of each single crystal has a hexagonal symmetry where the oxygen and hydrogen bonds, form hexagons. These so called base planes pile up with a constant distance of 0.737 nano-meters [[4]]. The main symmetry axis is perpendicular to the base planes and it is referred to as the crystal axis.There are two types of ice: the columnar ice and the granular ice. The columnar ice is the major consistent of river ice and first-year Arctic sea ice. Its microstructure is reminiscent of columnar zone of metallic ingots and results from unidirectional heat flow during the solidification. This type of ice is an orthotropic solid: it possesses three mutually perpendicular axes about which a rotation of 180° gives an identically appearing microstructure. Three variants are found in nature: S1, S2 and S3. The main difference is, if the crystallographic axes are randomly oriented or not.The granular ice, also called T1 ice, is the material of icebergs, ice islands, and polar glaciers. It also constitutes the upper layer of floating sheets of columnar ice. Its grain size typically ranges from 1 to 20mm, depending upon thermal-mechanical forming history. This type of ice is macroscopically isotropic [[3]].

5.3 Mechanical Behavior Of Ice
The ice can be considered as a material which mechanical behavior changes with strain rate. At low deformation rates, cracks do not form and the material is ductile. At high rates, cracks **do** initiate, the material is brittle independent of stress rate and it could be approximated by a linear elastic model with a failure criterion based on the maximum compressive strength. At intermediate strain rates, [[4]] cracks also develop, and the material is brittle under tension but ductile under compression. The ductile-brittle transition occurs at lower strain rates under tension because the applied stress opens the cracks directly. Under compression, the required tensile stress is generated locally through crack sliding. For this material (ice-sheet) deformed under these conditions, the low strain rate is less than 10^{-7} s^{-1} and the high strain rate is greater than 10^{-3} s^{-1}. From this perspective, during the

ice-structure interaction, the average effective strain rate within the contact zone is estimated from the relationship:

Strain rate= v/2L   (1)

Where v is the velocity of the ice relative to the structure, and L is the length of the structure.

5.4 Ice Properties From Environmental And Experimental Data

The majority of the data were taken from the Canadian Ice Service published in «The Sea Ice Climatic Atlas, East Coast of Canada 1971-2000». In this Atlas, there   are many charts for the ice concentration near the Canadian Atlantic coast [[5]]. Additional input was gathered from other researchers such as Sandwell [[6]], Johnston [[7]], Croasdale [[8]], Sand and Fransson [[9]] for the ice types, density, ice sheet size, thickness and velocity. The values used in the current work are presented in Table 2.

Table 2: Ice sheet parameters

Parameters	Values
Ice sheet size	Length =45 m and width=90m
Ice sheet thickness	0.6 m
Ice density	920 kg/m^3
Ice sheet velocity	0.3 m/s
Ice type	Granular

The mechanical properties (elasticity modulus, compressive strength etc) can be estimated by the experimental analysis from Timco and Frederking [[10]], and Petrovic [[11]] for granular ice, and are presented in Table 3.

Table 3: Mechanical properties of ice

Mechanical properties	Values
Behavior	Brittle isotropic elastic material
Elasticity modulus	6 GPa
Compressive Strength	4 MPa
Poisson ratio	0.33

VI. HYDRODYNAMIC LOADS

The hydrodynamic loads are the result of the sea waves and sea currents' action. As the Buffer Bell is positioned near the sea surface, it is experienced on surface waves and currents.The surface waves are simulated as regular waves and the sea currents act at the same direction with the sea waves. Two load case scenarios are investigated:

1)   The Ice sheet is moving straight to the BB which is stationary.
2)   The Ice sheet is moving straight to the BB which is oscillating due to the axial forces Fx (diffraction sea wave force) and D (hydrodynamic drag due to sea currents).

For the second load case scenario, due to the BB's size, only diffraction forces are occurred by the waves and drag force due to currents. For the diffraction loads, a numerical model was developed calculating the force versus the time [12]. The drag loads are based on the BB shape and skin friction.

$Fx=\pi*\rho*g*H*k*D^2*\cosh(k(z+h))*C_M*\cos(\omega t-\delta)/(8*\cosh(kh))$ (2)

$D=0.5*\rho*S*C_D*V^2$ (3)

The environmental conditions are summarized in table 4:

Table 4: Input data for hydrodynamic loads

Density ρ (kg/ m^3)	1028
Gravity acceleration g (m/s^2)	9.81
Wave Height H (m)	2.30
Regular wave length L (m)	58.0
Wave period (s)	6.08
Wavenumber k	0.1083
Floater Diameter D (m)	26
Operational Depth h (m)	2500
Submerged height z (m)	10
Hull height (m)	6.00
Inertia Coefficient C_M	2.00
Angular velocity ω (rad/s)	1.033

| Phase angle δ (rad)	-1.5708
Floater Drag coefficient C_D	1.2
Floater cross sectional area S (m^2)	156
Sea Current Velocity V (m/s)	0.3

The hydrodynamic forces were transformed to inertia acceleration, acting on the BB's center of gravity. The BB's mass distribution was considered (910 tons) and the results are summarized in table 5:

Table 5: Inertia Accelerations

Inertia acceleration (diffraction effect) (m/s^2)	$1.058*cos(1.033*t+1.5708)$
Inertia acceleration (drag effect) (m/s^2)	0.009516

VII. FINITE ELEMENT MODEL

The finite element analysis was performed by utilizing the LS-DYNA explicit finite element analysis code. LS-DYNA is a general purpose finite element code capable of analyzing the large deformation dynamic response of structures, with the main solution methodology based on explicit time integration[[13]]. Despite the fact that explicit solution was originally developed to solve high speed impact events, some particularities led to the necessity to use an explicit finite element code to solve a quasi-static event. More specifically, phenomena such as erosion of the ice sheet and the buffer bell material would not be possible without the use of explicit finite element analysis. Figure 5 represents the finite element model.
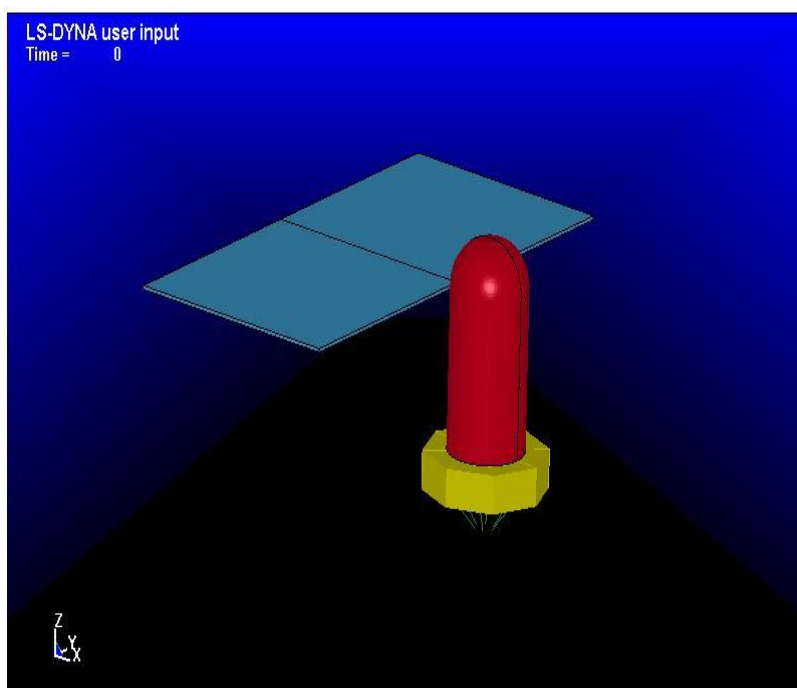
Figure 5: Finite element model

For this particular problem, the finite element model consisted of four parts:

7.1 The Mooring Lines
The mooring lines are made of dyneema, capable of absorbing large amounts of energy before fracture. From the modeling point of view, LS-DYNA offers a dedicated material model and element formulation for the modeling of cables. The material model suitable of modeling cables (*MAT_CABLE_DISCRETE_BEAM), can only be accompanied by a discrete beam/cable element formulation. The force F, generated by the cable is nonzero only if the cable is in tension. The force F is given by:

$$F = K \times max\,(\Delta L, 0) \qquad (2)$$

Where ΔL is the change in length
ΔL=current length –initial length   (3)

And the stiffness K is defined as:

$$K = \frac{E \times Area}{initial\ length}$$

(4)

Due to the fact that sudden application of the cable forces at the beginning of   the simulation can lead to excessive dynamic response of the cables, the application of the buoyancy forces was performed gradually. Table 4 summarizes the input properties used for dyneema mooring lines.

Table 6: Mooring lines mechanical properties

Density	ρ	1400 kg/m^3
Modulus of elasticity	E	46GPa
Cable diameter	D	96mm

7.2 The Floater
The floater (Figure 6) is made of high tensile steel (HTS). For the sake of computational efficiency due to the fact that no failure is expected in this area of the structure, linear elastic material model was used with typical mild steel properties, shown in Table 7. 3323 fully integrated 4-node shell elements were used to model this part.
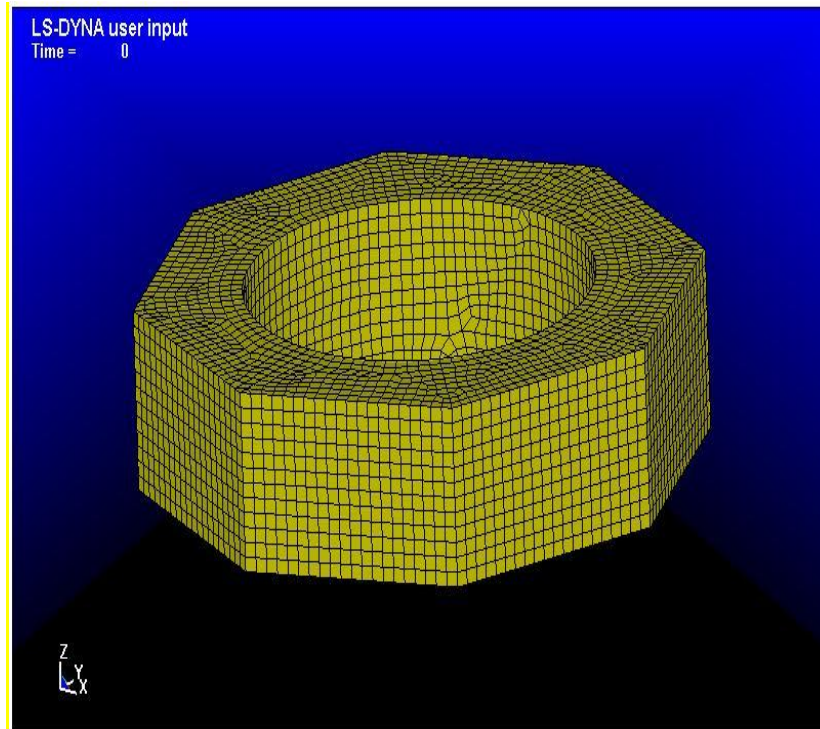
Figure 6: Floater finite element model

Table 7: Steel input properties

Density	ρ	7850kg/m^3
Modulus of Elasticity	E	200GPa
Poisson ratio	v	0.27

7.3 The Capacitor
The capacitor structure was modeled by 3477 fully integrated shell elements (Figure 6). An elastic-plastic material model was used with input properties summarized in the followingTable 8 was used for the aluminium capacitor load case. For the second load case of the Glass Reinforced Plastic (GRP), S-glass epoxy composite material was considered, with properties summarized in Table 9.
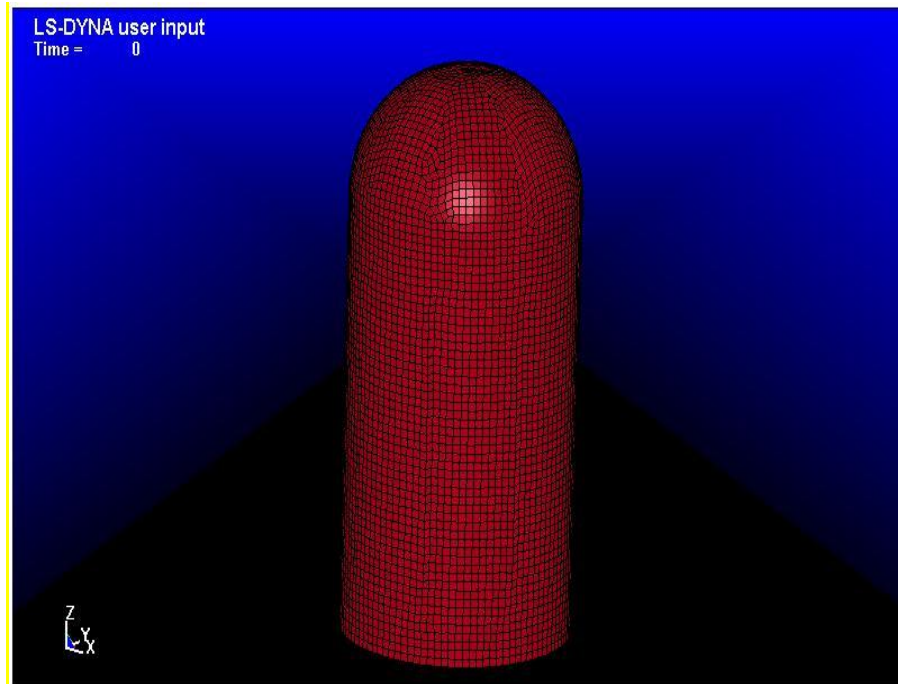
Figure 7: Capacitor finite element model

Table 8: Al5456 mechanical properties

Density	ρ	2770kg/m^3
Modulus of Elasticity	E	70GPa
Poisson ratio	v	0.33
Yield stress	S_y	255MPa
Ultimate stress	S_u	352MPa
Failure strain	ε_f	16%

Table 9: S-glass/epoxy material properties

| Density	ρ	1850 kg/m^3
Modulus of Elasticity	E_A	27.1 GPa
	E_B	27.1 GPa
	E_C	12.0 GPa
Poisson ratio	v_{BA}	0.11
	v_{CA}	0.11
	v_{CB}	0.18
Shear Modulus	G_{AB}	2.90 GPa
	G_{CB}	2.14 GPa
	G_{CA}	2.14 GPa
In plane Tensile Strength	S_{AT}	0.604 GPa
	S_{BT}	0.604 GPa
Out plane Tensile Strength	S_{CT}	0.058 GPa
Compressive Strength	S_{AC}	0.291GPa
	S_{BC}	0.291GPa
Matrix Mode Shear Strength	S_{AB}	0.075 GPa
	S_{BC}	0.075 GPa
	S_{CA}	0.058 GPa

7.4 Ice Sheet
The ice sheet (Figure 8) was modeled with 45000 8-node solid elements. Two elements across the thickness of the ice sheet were used leading to solid elements with dimensions of 0.3x0.3x0.3 m. An isotropic elastic material model was utilized with brittle failure option with input constants described in
Table 3 and Table 2.
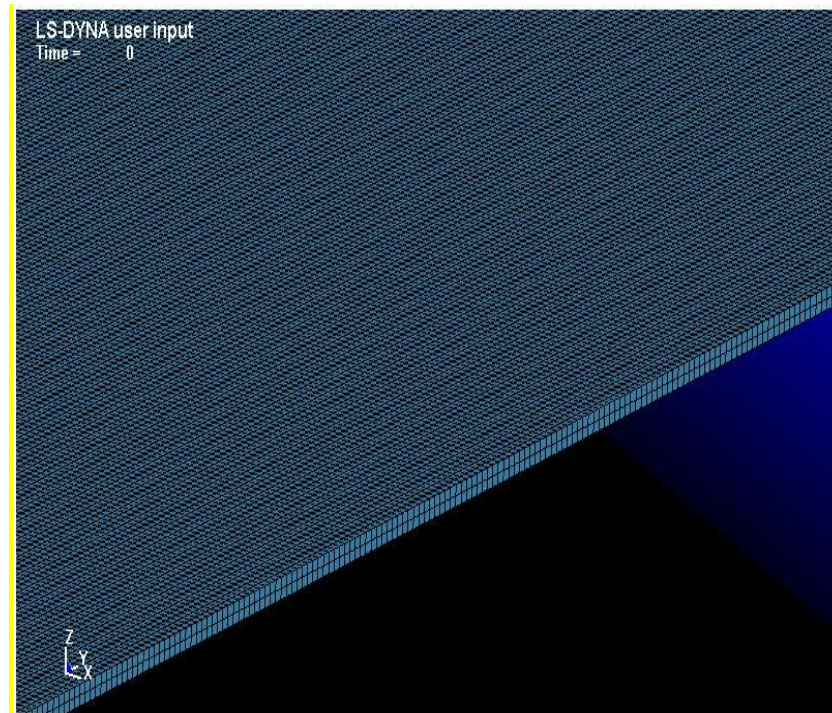
Figure 8: Ice sheet finite element model

6.5 Loads And Boundary Conditions
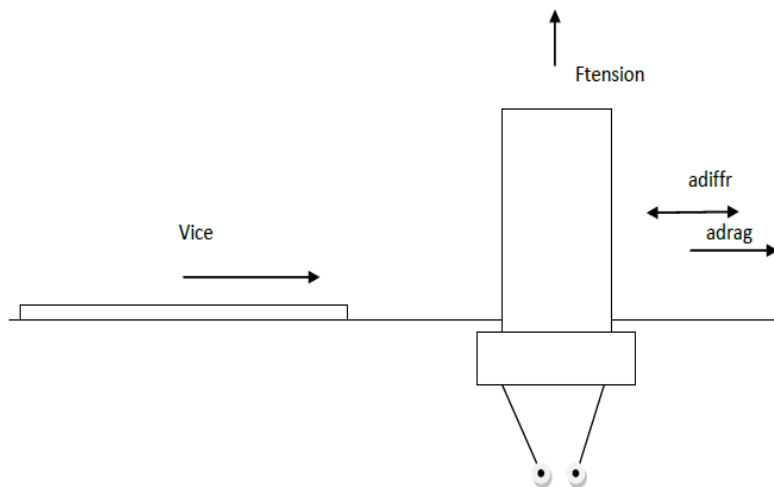
The lower ends of the mooring lines were clamped whereas the BB mass and buoyancy were applied to the structure as an inertia loads on the nodes in order to avoid stress concentration. A constant velocity of 0.3m/s was applied to the ice sheet. The hydrodynamic loads, described thoroughly in Section 6, where introduced as inertial nodal accelerations (for stationary BB load case, both (a_{diffr} and a_{drag}) inertia accelerationsare zero). Finally, in addition to the boundary conditions applied to the model, a contact algorithm was utilized to handle contact and erosion between the ice sheet and the buffer bell.

VIII.   RESULTS

In terms of the survivability of the structure, the most interesting results are the forces that are applied at the mooring lines because a possible failure of the mooring lines can lead to roll over of the buffer bell and a subsequent damage of the riser tube with direct environmental threats. The reaction forces versus time are depicted in Figures 9 and 10 for one of the mooring lines for each case study scenario. It can be seen that the forces applied on the mooring line will not lead to fracture of mooring lines (maximum load capacity 6700

kN)and the maximum value is experienced at the early stages of the simulation. At the later stages, the forces are reduced due to the reduction of the kinetic energy of the ice sheet due to erosion and subsequent reduction of its mass.At the case of the Oscillating BB, for both material case study scenarios, it can be observed that the generated forces at the mooring lines are almost the same for both cases, due to the similarity of the structure's mass. For the stationary BB case, the force oscillation is damped normally due to LS-Dyna contact algorithm. At the case of oscillatory BB, the impact is more steep leading to an oscillation with sea wave's frequency. Due to the BB rebound after the impact and the LS-Dyna's contact algorithm, the steep motion is damped leading to a constant load (after the 50 sec) at the mooring lines.
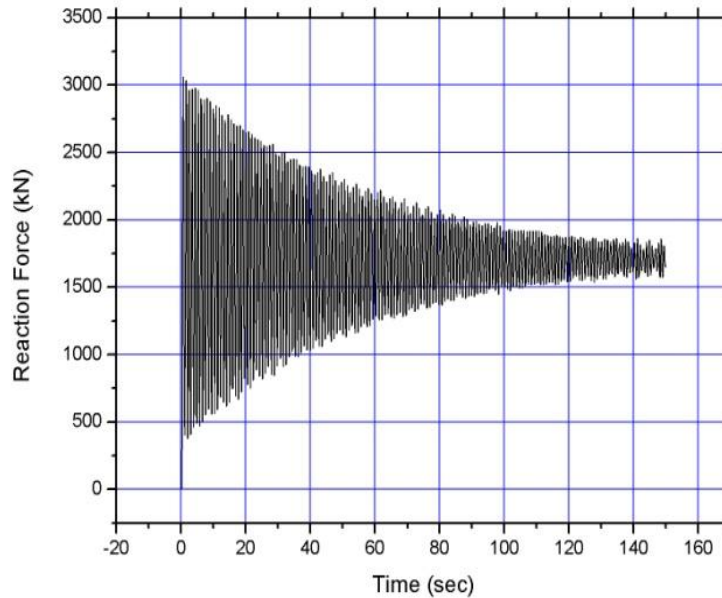

Figure 9: Force (kN) versus time applied on the mooring lines for stationary BB.
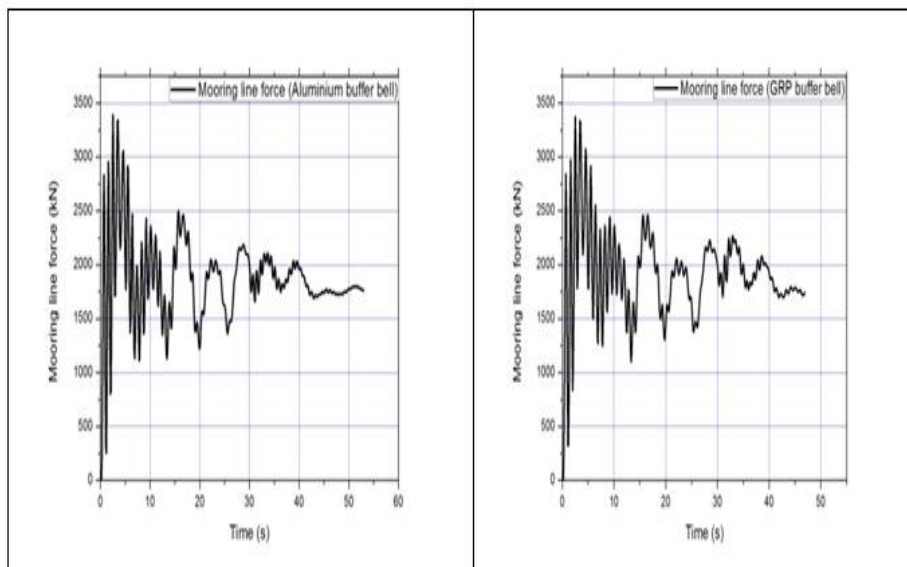

Figure 10: Force (kN) versus time applied on the mooring lines for oscillating (aluminum and GFRP) BB.

Another important aspect of the results is the damage induced on the buffer bell's capacitor structure. Possible failure will lead to oil leakage when the structure starts to operate and repair techniques must be provisioned. Regarding the aluminum capacitor, for the stationary BB case study scenario, a rupture is occurred which leads to a hole of 1x1m approximately (Figures 11-13). For the oscillating BB case study scenario, a large opening is

observed, with an opening of approximately 4 m in diameter and a large zone of developed plastic strain (Figure 14). This condition does not threat the survivability of the structure, but the oil leakage is certain. In addition, extensive repair techniques have to be established interrupting the BB's installation for more than 15 days.
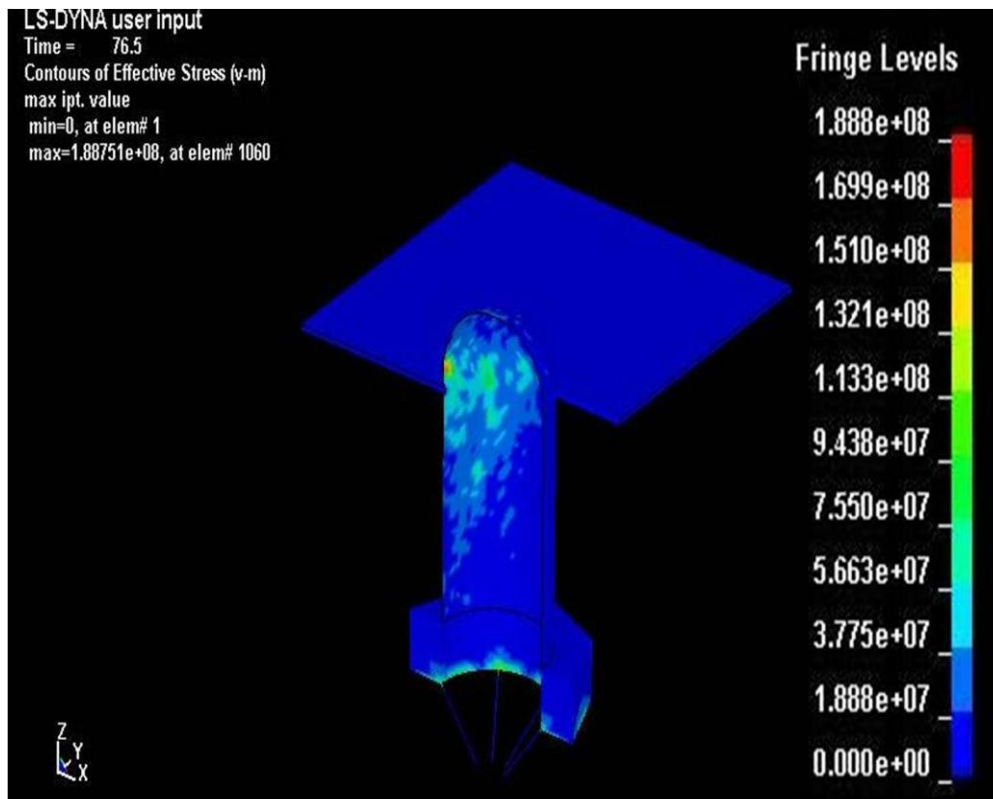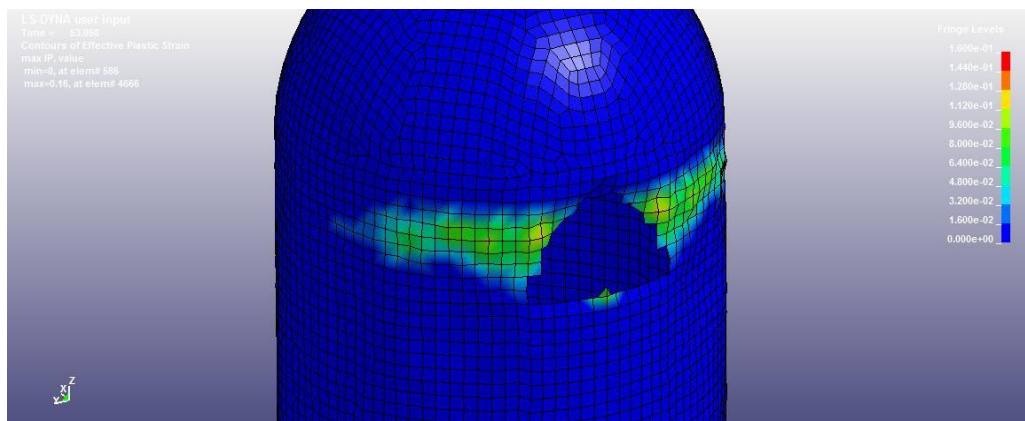

Figure 11: Von-mises stresses applied on the structure at time 76.5sec (Stationary BB)
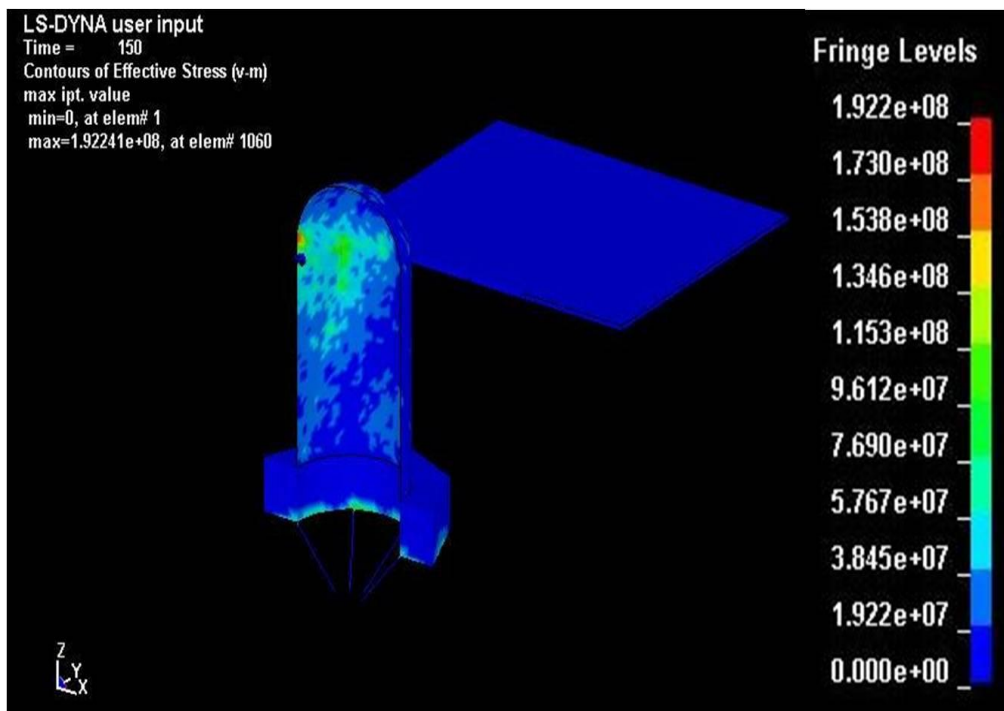
Figure 12: Von-mises stresses applied on the structure at 150sec, after some of the elements in impact have failed. (Stationary BB)
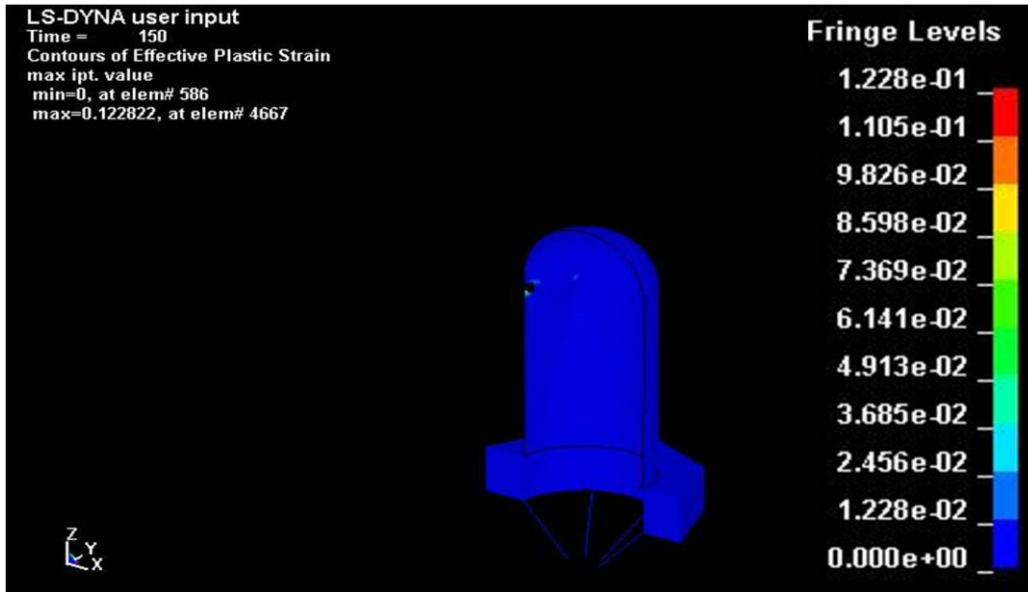
Figure 13: Plastic strain induced on the structure at 150sec (Stationary BB)

Figure 14: Plastic strain and failure of the aluminum capacitor (Oscillating BB)

The change of capacitor's manufacturing material was introduced as an optimized solution for the Ice-structure interaction case study scenario.Regarding the GFRP design, the damage is significantly reduced, leading to an eroded area less than 1.0 m in diameter and significantly smaller damage, as seen in Figure 15. Concerning the repair methods, this damaged area can be fixed within 10 days, reducing the delays on the BB's installation.
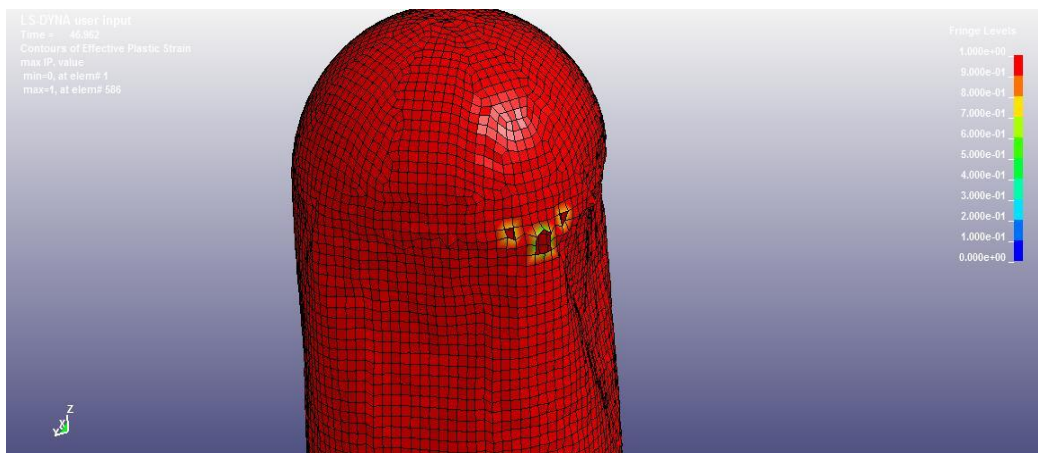
Figure 15: Failure and deformation observed at the GRP capacitor structure (Oscillating BB)

IX.   CONCLUSIONS

In this paper, an extensive research on ice sheets characteristics and hydrodynamic loads was performed.A finite element analysis has been also performed in order to estimate the damage on the capacitor structure for the load case of an impact with an ice sheet during the deployment phase. Two load cases were investigated: a) stationary and b) oscillating BB. The Aluminum Capacitor was replaced by a GFRP capacitor as an optimized solution for the ice-structure interaction. The GFRP Capacitor was proved to have a better repair strategy, reducing the BB's installation delay. Additionally, no failure of the mooring lines is expected and the safety of the structure is not compromised.The mooring lines also carried, a little bit greater forces than in the case of no waves/drag loads [14],[15]. Future work will include the further increase of hydrodynamic loads (higher wave heights), investigating the maximum load capacity of the GFRP Capacitor.

REFERENCES

[1].   Hamn-Ching Chen, Chia-Rong Chen and Richard S. Mercier, 2006, 'CFD Simulation of Riser VIV' , Minerals Management Service, MMS Project number 481
[2].   Project FP-6516360 "DIFIS", D8.1, 2006, 'Report on Deployment. Recovery Procedure'
[3].   Erlad M. Schulson, 2000, 'Brittle failure of ice', Pergamon, Enginnering Fracture Mechanics 68 (2001) 1839-1887
[4].   G.W. Timco, 1979, 'The mechanical and morphological properties of ice', Port and Ocean Engineering under Arctic conditions
[5].   A. Derradji-Aouat and M. Lau, (2005), 'Ice loads on Electric Power Generating Stations in BelleIsleStrait', Proc., 18th Int. Conf. on Port and Ocean Eng. Under Arctic Conditions, Vol I, pp.387-398
[6].   Sandwell Inc, 1998, 'Ice regimes off the West Coast of Newfoundland', PERD/ CHC Report 20-35
[7].   Johnston M., 1999, 'Field Study of Ice Characteristics off the West Coast of Newfoundland', PERD/ CHC Report 2-67
[8].   Croasdale K.R & Associates Ltd, 1999, 'Field Study of Ice Characteristics off the West Coast of Newfoundland', PERD/ CHC Report 2-70
[9].   Bjonar Sand and Lennart Fransson, 2006, 'Nonlinear finite element simulations of ice sheet forces on conical structures', OMAE2006-92520, 25th International Conference on Offshore Mechanics and Arctic Engineering, Hamburg, Germany
[10].   G.W. Timco and R.M.W. Frederking, 1984, 'An investigation of the failure envelope of granular/discontinuous-columnar sea ice', Elsevier Science Publishers, Cold Regions Science and Technology, 9, pp. 17-27
[11].   J.J. Petrovic, 'Mechanical Properties of Ice and Snow', 2003, Journal of materials science 38, pp 1-6
[12].   B. Multu Sumer, Jorgen Fredsoe, "Hydrodynamics Around Cylindrical Structures", World Scientific, Revised Edition, 2006.
[13].   LS-DYNA Users Manual 2007 Version 971, LSTC, ISBN 0-9778540-2-7
[14].   D. Mazarakos, A.Kotzakolios, F. Andritsos and V. Kostopoulos, 2010, 'Ice Loading Analysis of Underwater Structure Dedicated to the Intervention and Remediation of Trapped Pollutant in Tanker Wrecks', 5th International ASRANET conference.
[15].   D. Mazarakos, A.Kotzakolios, and V. Kostopoulos, 2014, 'Ice Impact Analysis of a Metallic and Composite Underwater Structure Dedicated to the Intervention and Remediation of Trapped Pollutant in Tanker Wrecks', 7th International ASRANET conference.